J|A|C|S
ARTICLES

Published on Web 04/16/2010

Nacre Protein Fragment Templates Lamellar Aragonite Growth

Rebecca A. Metzler,[†] John Spencer Evans,[‡] Christopher E. Killian,[†,§] Dong Zhou,[†] Tyler H. Churchill,[†] Narayana P. Appathurai,[||] Susan N. Coppersmith,[†] and P. U. P. A. Gilbert*[,†]

Department of Physics, University of Wisconsin—Madison, 1150 University Avenue, Madison, Wisconsin 53706, Center for Biomolecular Materials Spectroscopy, Laboratory for Chemical Physics, New York University, 345 East 24th Street, New York, New York 10010, Department of Molecular and Cell Biology, University of California, Berkeley, California 94720, and Synchrotron Radiation Center, 3731 Schneider Drive, Stoughton, Wisconsin 53589

Received November 16, 2009; E-mail: pupa@physics.wisc.edu

Abstract: Proteins play a major role in the formation of all biominerals. In mollusk shell nacre, complex mixtures and assemblies of proteins and polysaccharides were shown to induce aragonite formation, rather than the thermodynamically favored calcite (both aragonite and calcite are $CaCO_3$ polymorphs). Here we used N16N, a single 30 amino acid−protein fragment originally inspired by the mineral binding site of N16, a protein in the nacre layer of the Japanese pearl oysters (*Pinctada fucata*). In a calcite growth solution this short peptide induces in vitro biomineralization. This model biomineral was analyzed using X-ray PhotoElectron Emission spectroMicroscopy (X-PEEM) and found to be strikingly similar to natural nacre: lamellar aragonite with interspersed N16N layers. This and other findings combined suggest a hypothetical scenario in which in vivo three proteins (N16, Pif80, and Pif97) and a polysaccharide (chitin) work in concert to form lamellar nacre.

Introduction

Bones, teeth, and shells are fascinating biomineral composites of proteins, polysaccharides, and minerals.[1] The organic matrices are usually the minority components in non-vascularized biominerals, ranging between 2−5 wt %[2] and 0.1 wt %.[3] These low concentrations imply that the mineral-associated proteins work very efficiently for the organisms, which are able to form the entire biomineral mass while transmitting down the lineage information on how to synthesize only a small wt % of the final product. Such genetic efficiency, combined with the excellent mechanical properties of all biominerals, explains the evolutionary advantage of adopting biomineral skeletons, which enabled the Cambrian explosion of animal diversity.[1,4]

Despite the success of biominerals in nature, specific functions of biomineral proteins are hard to identify due to a number of factors, including our inability to probe the molecular-level interactions that occur between proteins and minerals, the complex environments that exist in vivo,[5−7] and the possibility that cooperative protein participation is necessary for biomineral formation. In addition, no biomineral proteins have thus far been crystallized; therefore, their structure cannot be solved by diffraction.

Mollusk shell nacre, or mother-of-pearl, is one of the most studied biominerals, with many proteins already isolated and sequenced[8−11] and a few protein functions identified.[12−17] Nacre is an iridescent, lamellar material in which organic matrix layers containing chitin and proteins alternate with aragonite, the orthorhombic polymorph of $CaCO_3$. In vitro growth of $CaCO_3$ normally produces calcite, the trigonal $CaCO_3$ polymorph thermodynamically favored, unless additives are introduced in

* Previously published as Gelsomina De Stasio.
† University of Wisconsin—Madison.
‡ New York University.
§ University of California.
|| Synchrotron Radiation Center.

(1) Lowenstam, H. A.; Weiner, S. *On Biomineralization*; Oxford University Press: Oxford, 1989.
(2) Hare, P. E.; Abelson, P. H. *Carnegie Institution of Washington Yearbook* **1965**, *64*, 223–234.
(3) Wilt, F. *Journal of Structural Biology* **1999**, *126*, 216–226.
(4) Stanley, S. M. *Earth Systems History*; W. H. Freeman & Co.: New York, 2005.
(5) Falini, G.; Albeck, S.; Weiner, S.; Addadi, L. *Science* **1996**, *271*, 67–69.
(6) Belcher, A. M.; Wu, X. H.; Christensen, R. J.; Hansma, P. K.; Stucky, G. D.; Morse, D. E. *Nature* **1996**, *381*, 56–58.
(7) Li, H. Y.; Estroff, L. A. *J. Am. Che. Soc.* **2007**, *129*, 5480–5483.
(8) Mann, K.; Weiss, I.; André, S.; Gabius, H. J.; Fritz, M. *Eur. J. Biochem.* **2001**, *267*, 5257–5264.
(9) Shen, X.; Belcher, A. M.; Hansma, P. K.; Stucky, G. D.; Morse, D. E. *J. Biol. Chem.* **1997**, *272*, 32472–32481.
(10) Michenfelder, M.; Fu, G.; Lawrence, C.; Wustman, B. A.; Taranto, L.; Evans, J. S.; Morse, D. E. *Biopolymers* **2003**, *70*, 522–533.
(11) Zhang, C.; Li, S.; Z., M.; Xie, L.; Zhang, R. *Marine Biotechnol* **2006**, *8*, 624–633.
(12) Suzuki, M.; Saruwatari, K.; Kogure, T.; Yamamoto, Y.; Nishimura, T.; Kato, T.; Nagasawa, H. *Science* **2009**, *325*, 1353–1390.
(13) Weiss, I. M.; Kaufmann, S.; Mann, K.; Fritz, M. *Biochem Biophys Res Com* **2000**, *267*, 17–21.
(14) Cariolou, M. A.; Morse, D. E. *J. Comp. Physiol. B* **1988**, *157*, 717–729.
(15) Yan, Z.; Jing, G.; Gong, N.; Li, C.; Zhou, Y.; Zhang, R. *Biomacromol* **2007**, *8*, 3597–3601.
(16) Fu, G.; Valiyaveettil, S.; Wopenka, B.; Morse, D. E. *Biomacromol* **2005**, *6*, 1289–1298.
(17) Kono, M.; Hayashi, N.; Samata, T. *Biochem Biophys Res Com* **2000**, *269*, 213–218.

 © 2010 American Chemical Society

	24	25	26	27	28	29	30	31	32	33	34	35	36	37	38	39	40	41	42	43	44	45	46	47	48	49	50	51	52	53
n16N	A	Y	H	K	K	C	G	R	Y	S	Y	C	W	I	P	Y	D	I	E	R	D	R	Y	D	N	G	D	K	K	C
n16NN	A	Y	H	K	K	C	G	R	Y	S	Y	C	W	I	P	Y	N	I	Q	R	N	R	Y	N	N	G	N	K	K	C

	1	2	3	4	5	6	7	8	9	10	11	12	13	14	15	16	17	18	19	20
n16-1	M	K	C	T	L	R	W	T	I	T	A	L	V	L	L	G	I	C	H	L
n16-2																				
n16-3		T																		
pearlin		T																		

	21	22	23	24	25	26	27	28	29	30	31	32	33	34	35	36	37	38	39	40
n16-1	A	R	P	A	Y	H	K	K	C	G	R	Y	S	Y	C	W	I	P	Y	D
n16-2																				
n16-3					F	R	T													
pearlin					F	R	T													

	41	42	43	44	45	46	47	48	49	50	51	52	53	54	55	56	57	58	59	60
n16-1	I	E	R	D	R	Y	D	N	G	D	K	K	C	C	F	C	R	Y	A	W
n16-2						R				G								N		
n16-3																				
pearlin																		N		

	61	62	63	64	65	66	67	68	69	70	71	72	73	74	75	76	77	78	79	80
n16-1	S	P	W	Q	C	N	E	E	E	R	Y	E	W	L	R	C	G	M	R	F
n16-2						K		D										H	K	
n16-3								D										H	K	
pearlin								D										H	K	

	81	82	83	84	85	86	87	88	89	90	91	92	93	94	95	96	97	98	99	100
n16-1	Y	S	L	C	C	Y	T	D	D	D	N	G	N	G	N	G	N	G	N	G
n16-2		Y	M												D					x
n16-3		Y	M																	x
pearlin		Y	M																	

	101	102	103	104	105	106	107	108	109	110	111	112	113	114	115	116	117	118	119	120
n16-1	N	G	L	N	Y	L	K	S	L	Y	G	G	Y	G	N	G	N	G	E	F
n16-2	x		F																	
n16-3	x		F																	
pearlin			F																	

	121	122	123	124	125	126	127	128	129	130	131
n16-1	W	E	E	Y	I	D	E	R	Y	D	N
n16-2											K
n16-3											K
pearlin											K

Figure 1. (Top) 30-amino acid sequence of the N16N and N16NN peptides. The negatively charged Asp and Glu amino acids (D and E) are highlighted in red, while their charge-neutral analogues Asn and Gln (N and Q) are highlighted in green. The N16N peptide is expected to be biomineral active in that its five negative charges are expected to bind to Ca^{2+} in $CaCO_3$. The N16NN peptide is not expected to bind and, in fact, was prepared to test the charge-based binding hypothesis. The N16N peptide is sequenced after a domain close to the N-terminus amino acids 24−53, highlighted in orange, of the N16-1 protein extracted from *Pinctada fucata* shell nacre, which is one of three proteins in the N16 family. (Bottom) Sequences of the three proteins in the N16 family, along with the pearlin protein, which was extracted from the *P. fucata* pearl nacre, and is identical in sequence to N16-3, except for the amino acid at position 58.[38,39]

the growth solution.[18] However, several studies have shown that aragonite is formed in vitro using mixtures of proteins extracted from nacre either in the absence of chitin[6,19] or in the presence of chitin.[5,12]

In this work, we used a reductionist approach: a single 30-amino acid peptide, N16N, sequenced after the protein domain previously identified as the mineral-binding site of the N16-1 protein, and calcium carbonate. The N16-1 protein is one of three N16 proteins extracted from the water-insoluble matrix of the nacreous layer in the bivalve *Pinctada fucata*, also known as the Japanese pearl oyster, and has a sequence similar to that of the pearl protein pearlin.[19,20] The N16N peptide is rich in aspartate and glutamate residues.[19,21] The protein sequences are presented in Figure 1.

In a previous experiment, Metzler et al. observed distinct effects on the X-ray absorption spectroscopy of N16N upon binding with calcite in vitro. These effects were absent when the Asp and Glu residues were replaced in the sequence by their charge-neutral equivalents, Asn and Gln; the charge-neutral peptide was termed N16NN,[21,22] thus confirming that Asp and Glu are indeed active at the organic−mineral interface.[22]

In the present study, we show that the N16N peptide self-assembles into layers and promotes aragonite growth in lamellar crystals. Aragonite polymorph selection and self-assembly are not observed in the control N16NN system.

The in vitro crystal growth experiments, which were intentionally kept as simple as possible, do not reproduce many of the factors that are present in vivo, including the following: many proteins are present;[1] there is a three-dimensional organic scaffold in which biomineral formation takes place;[5] the

(18) Meldrum, F. C.; Hyde, S. P. *J. Cryst. Growth* **2001**, *231*, 544–558.
(19) Samata, T.; Hayashi, N.; Kono, M.; Hasegawa, K.; Horita, C.; Akera, S. FEBS Lett. 1999, *462*.
(20) Miyashita, T.; Takagi, R.; Okushima, M.; Nakano, S.; Miyamoto, H.; Nishikawa, E.; Matsushiro, A. *Marine Biotechnol* **2000**, *2*, 409–418.
(21) Collino, S.; Evans, J. S. *Biomacromol* **2008**, *9*, 1909–1918.
(22) Metzler, R. A.; Kim, I.; Delak, K.; Evans, J.; Zhou, D.; Beniash, E.; Wilt, F.; Abrecht, M.; Chiou, J.-W.; Guo, J.; Coppersmith, S.; Gilbert, P. U. P. A. *Langmuir* **2008**, *24*, 2680–2687.

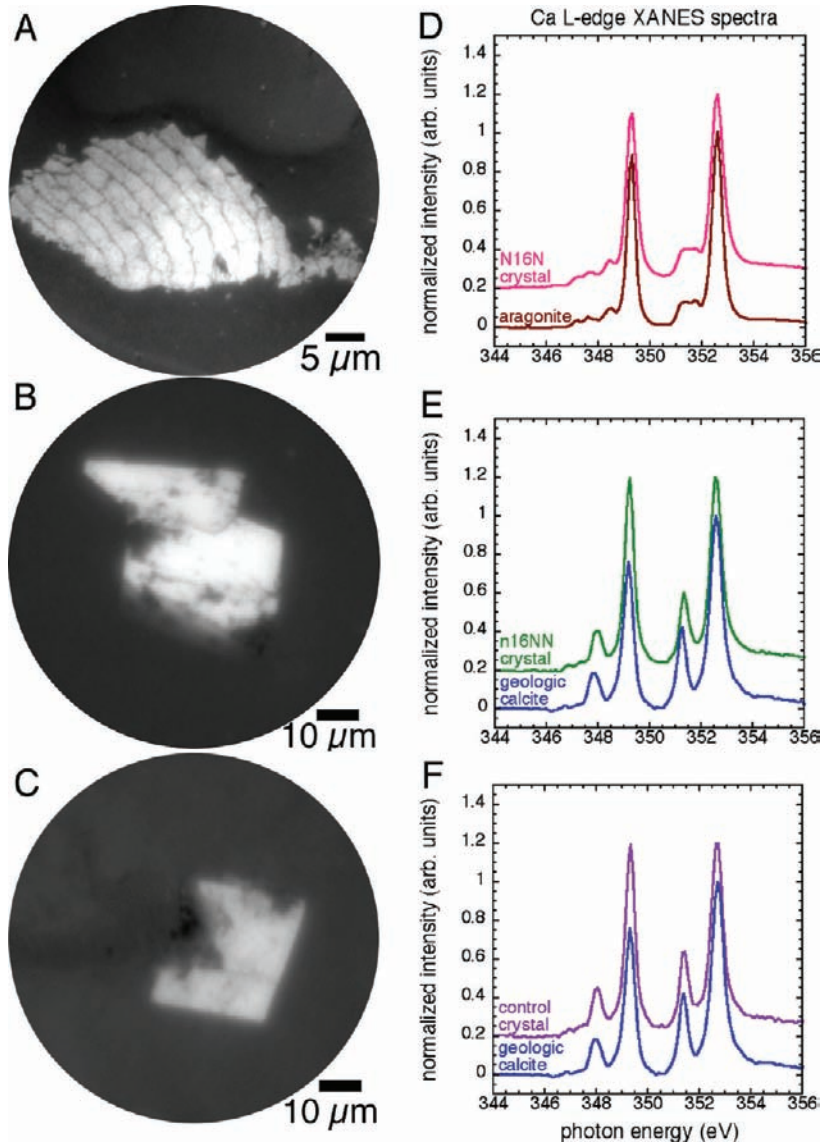

Figure 2. (A−C) X-PEEM calcium maps obtained by a digital ratio of 352.6 and 344 eV images of a crystal grown from solution in the presence of (A) N16N, (B) N16NN, (C) and no peptide. All crystals were embedded in epoxy and polished; therefore, the crystal surfaces were flat. Notice the outlines of the three crystals, revealing the crystal habit. B and C are recognizably rhombohedra with missing mineral where the Kevlar threads were located during crystal growth, while A is not. A shows a lamellar aragonite crystal, in which aragonite lamellae alternate with low-Ca layers (dark lines in A). These lines identify layers occluded during crystal growth and observed in cross-section in A. (D−F) Calcium L-edge X-ray absorption near-edge structure (XANES) spectra extracted from the crystals in A−C. In D we also report a spectrum from geologic aragonite and calcite in E and F. Clearly, the crystal grown in the presence of N16N is aragonite, while the control crystals are calcite.

chemical environment for biomineralization is complex and the extrapallial fluid may play a key role, as suggested by many authors,[23,24] although not others.[25] We cannot, therefore, conclude that the aragonite polymorph selection observed in vitro using the N16N peptide directly identifies the in vivo protein function. We can, however, state with confidence that aragonite polymorph selection and lamellar structure occur in the simplest of biominerals: a single short peptide and calcium carbonate.

We also present the results of spectroscopic experiments on nacre from *Pinctada fucata*, which demonstrate that aragonite growth occurs before the onset of the lamellar nacre structure.

Results

The N16N self-assembly and aragonite polymorph selection are shown by X-ray PhotoElectron Emission spectroMicroscopy (X-PEEM) data. Figure 2 presents calcium maps and X-ray absorption spectra acquired on three crystals grown in vitro from a calcite-growth solution in the presence of 100 μM N16N or 100 μM N16NN or in the absence of any peptides. The solution contained 10 mM $CaCl_2$ and was exposed to carbonate ions from volatile ammonium carbonate.[26] The Ca maps in Figure

(23) Wilbur, K. M.; Bernhardt, A. M. *Biology Bulletin* **1984**, *166*, 251–259.
(24) Ma, Z.; Huang, J.; San, J.; Wang, G.; Li, C.; Xie, L.; Zhang, R. *J. Biol. Chem.* **2007**, *282*, 23253–23263.
(25) Addadi, L.; Joester, D.; Nudelman, F.; Weiner, S. *Chem.—Eur. J.* **2005**, *12*, 980–987.
(26) Addadi, L.; Moradian, J.; Shay, E.; Maroudas, N. G.; Weiner, S. *Procs. Natl. Acad. Sci. USA* **1987**, *84*, 2732–2736.

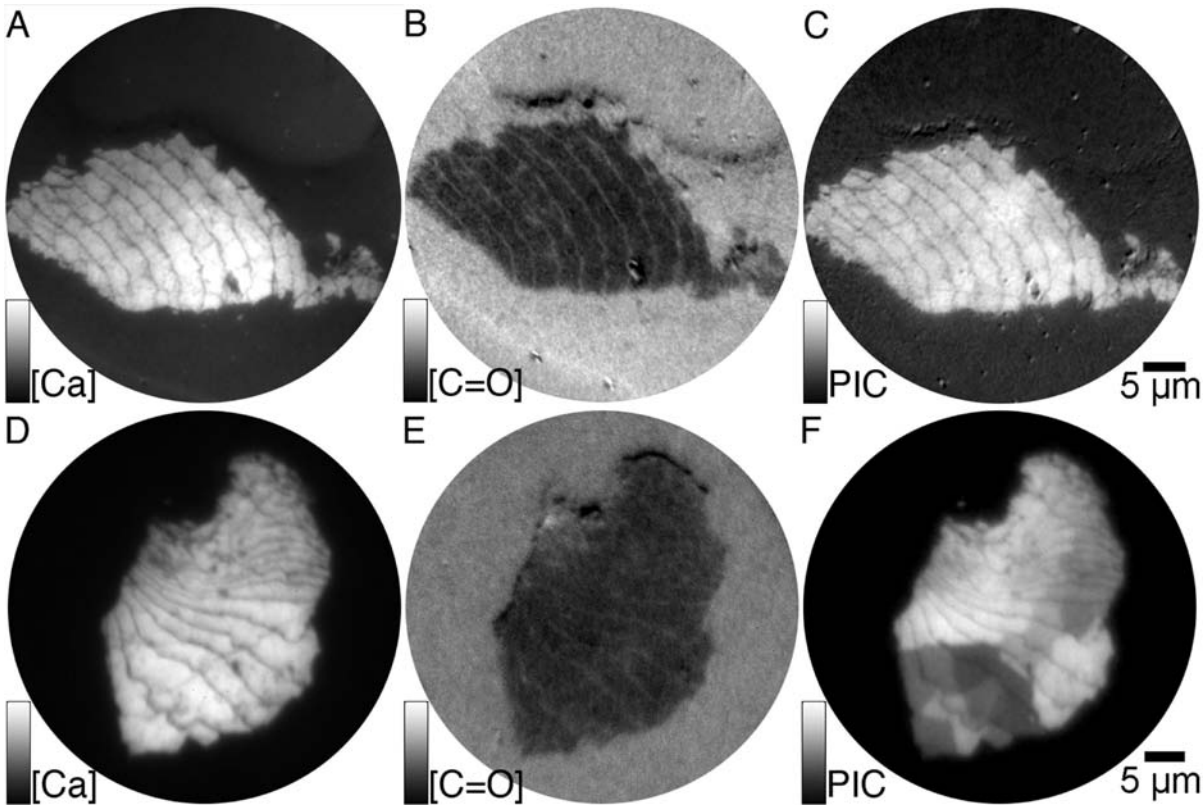

Figure 3. (A−C) X-PEEM maps obtained on the same lamellar N16N−aragonite crystal in Figure 1A. (D−F) X-PEEM maps obtained on another lamellar N16N−aragonite crystal. (A) Calcium distribution map obtained by ratio of 352.6 and 344 eV images, the calcium L_2 peak and pre-edge, respectively, showing high [Ca] in the aragonite lamellae and low-Ca in N16N layers. (B) Carbon distribution map obtained by ratio of images taken on the amide and carboxylate peak (288.2 eV) characteristic of the peptide bond between amino acids and at the pre-edge (280 eV). The map shows that the layers (light gray level) occluded in the aragonite crystal (dark gray level) are rich in peptide bonds, thus indicating that the layers are self-assembled N16N. (C) A polarization-dependent imaging contrast (PIC) map obtained by digital ratio of 290.3 and 280 eV images (the carbonate π^* peak, and pre-edge). Aragonite crystals with different *c*-axis orientations with respect to the X-ray polarization vector result in different gray levels within the map. Notice that the crystal lamellae exhibit a uniform gray level; therefore, they are co-oriented with respect to their c-axes. PIC does not detect rotations in the *a*- and *b*-axes; therefore, the crystallites within the crystal could be misoriented in the *ab*-plane. (D) [Ca] map from another lamellar aragonite crystal from an independent preparation, fully consistent with that in A. (E) [C═O] map fully consistent with that in B. (F) PIC map showing differences in gray level within the aragonite lamellae, indicating different *c*-axis orientations.

2 clearly show high concentration of calcium in the $CaCO_3$ crystals. In the presence of N16N the crystal habit departs from the rhombohedra observed in the presence of N16NN and the control. The N16N-exposed crystal also shows low-Ca layers occluded within the crystal. The only non-Ca component in the model biomineral system is N16N, so it is natural to infer that these layers are self-assembled N16N (further evidence for this is presented in Figure 3).

The spectra in Figure 2 show that the crystal grown in the presence of N16N is aragonite, while the other two crystals are calcite. This is a significant result since the calcite polymorph is thermodynamically favored when crystal growth occurs in a $CaCl_2$ solution with ammonium carbonate diffusion at ambient temperature, as done here. This indicates that the N16N peptide alone stabilizes the aragonite polymorph during crystal growth.

The maps of Figure 3 show that the layers interspersed with lamellar aragonite are organic and rich in amide and carboxylate, as expected for all peptide bonds in proteins and peptides. Because the growth solution contained only water, Ca^{2+}, Cl^-, and CO_3^- ions, Kevlar (polyimide) threads, and N16N, and specifically no other proteins, we conclude that the layers occluded in lamellar aragonite crystals are composed of self-assembled N16N layers. Figure 3C shows that the aragonite lamellae are all co-oriented along their *c*-axes, while Figure 3F shows various *c*-axis orientations as revealed by different gray levels in polarization-dependent imaging contrast (PIC).[27−30] Whether the *c*-axes are co-oriented or not, the crystallites maintained their *c*-axis orientation even when they were growing through N16N layers; thus, we infer that the N16N layers are not continuous but porous. All crystals grown in the absence of N16N or in the presence of N16NN were homogeneous calcite rhombohedra, with no lamellar structure, as those in Figure 2B,C.

The results of Figures 2 and 3 are difficult to reproduce, as they only occur in a small subset of the experiments (5%), as explained in the Supporting Information and below.

Figure 4 shows the PIC map and spectra acquired at the nacre-prismatic boundary of *P. fucata*. Two large blocks of aragonite are observed at the organic boundary, which have different

(27) Politi, Y.; Metzler, R. A.; Abrecht, M.; Gilbert, B.; Wilt, F. H.; Sagi, I.; Addadi, L.; Weiner, S.; Gilbert, P. U. P. A. *Procs Natl Acad Sci USA* **2008**, *105*, 17362–17366.
(28) Metzler, R. A.; Abrecht, M.; Olabisi, R. M.; Ariosa, D.; Johnson, C. J.; Frazer, B. H.; Coppersmith, S. N.; Gilbert, P. U. P. A. *Phys. Rev. Lett.* **2007**, *98*, 268102.
(29) Gilbert, P. U. P. A.; Metzler, R. A.; Zhou, D.; Scholl, A.; Doran, A.; Young, A.; Kunz, M.; Tamura, N.; Coppersmith, S. N. *J. Am. Chem. Soc.* **2008**, *130*, 17519–17527.
(30) Killian, C. E.; Metzler, R. A.; Gong, Y. T.; Olson, I. C.; Aizenberg, J.; Politi, Y.; Addadi, L.; Weiner, S.; Wilt, F. H.; Scholl, A.; Young, A.; Coppersmith, S. N.; Gilbert, P. U. P. A. *J. Am. Chem. Soc.* **2009**, *131*, 18404–18409.

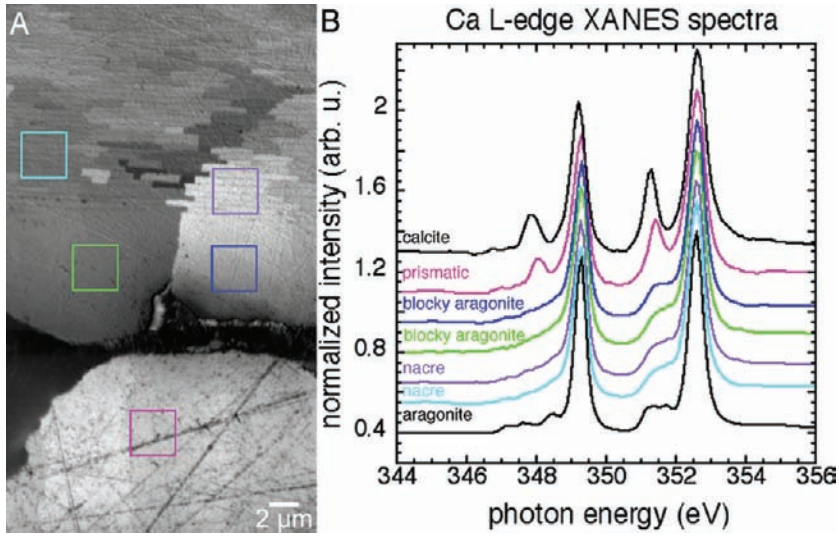

Figure 4. PIC maps and Ca spectra taken at the prismatic-nacre boundary in *P. fucata*. (A) PIC map showing one prism at the bottom and a dark wall of organic molecules separating the calcite from aragonite compartments. Immediately above this organic wall two large and blocky aragonite crystals are observed, and approximately 8 μm above, the familiar lamellar nacre appearance begins, and continues for several millimeters (not shown). Notice that the gray levels of the two large aragonite crystals are different, indicating that their *c*-axes are not parallel. Interestingly, their crystal orientations propagate into the nacre lamellae, as these grow across the organic matrix layers. At a greater distance from the onset of lamellar nacre formation, much greater *c*-axis co-orientation is observed. (B) Ca spectra extracted from the correspondingly colored regions in A. For reference, spectra from geologic aragonite and calcite are also presented in black. The spectrum from the prism (magenta) is calcite and those from the two large blocky aragonite crystals (green and blue) are aragonite, as are the nacre spectra (cyan and purple).

c-axis orientations, and grow for approximately 8 μm, until the onset of lamellar nacre formation. Remarkably, the crystal *c*-axis orientation propagates through the nacre organic matrix layers, because these are porous.[31] The high contrast shown in these first few nacre lamellae rapidly decays, and all aragonite tablets become more co-oriented as nacre growth progresses. This ordering in *P. fucata* sheet nacre is much more rapidly ($\sim$10 μm) achieved than in *Haliotis rufescens* ($\sim$50 μm).[29] Perfect co-orientation, however, is never observed in nacre from any shell. Consistent with previous observations by diffraction[32] and PIC mapping,[29] in these PIC maps nacre tablets behave as single crystals of aragonite.

Discussion

Remarkably, the minimalist aragonite lamellar biomineral produced in vitro here is reminiscent of natural mollusk shell nacre (PIC maps in Figures 3 and 4), suggesting that lamellar self-assembly of N16N−aragonite is a possible function of the N16 protein in vivo.

One function that N16N does *not* have is directing crystal orientation, as shown in Figure 3. The majority of the lamellar crystals show aragonite crystals with highly co-oriented c-axes, but others do not, as the one shown in Figure 3F. The crystal orientation propagation through organic layers appears to occur similarly in natural nacre and lamellar N16N−aragonite, and is nicely interpreted with the mineral bridges through porous organic layers, as first reported by Schäffer et al.[31]

The observed thickness of the N16N layers in lamellar aragonite crystals varies between 200 and 600 nm, indicating that the N16N does not self-assemble as a single-molecule layer but as multimolecular layers. The propensity for aggregation that N16N exhibits suggests that in vivo N16 may aggregate with other proteins, which were not present in the in vitro experiment.

Elegant work by Suzuki et al. showed that the Pif80 and Pif97 complex binds aragonite in vivo, Pif97 alone binds chitin, and the complex of Pif80, Pif97, and N16 promotes aragonite growth in vitro in the presence of chitin.[12] Using immunolabeling, they also showed that Pif80 is present in high concentration at the organic boundary and throughout lamellar nacre. Surprisingly, Suzuki et al. showed that when Pif80 (the non-chitin-binding protein) is knocked out, the nacre lamellae are no longer assembled.[12] Keene et al. showed that the N16N peptide is also chitin binding.[33] The spectra of Figure 4 show that at the organic boundary the first mineral formed is blocky aragonite, thus supporting the conclusion by Suzuki et al. that Pif80 promotes aragonite formation. All these observations combined raise a possible scenario, in which Pif80 acts first, and only $\sim$8 μm later, at the onset of lamellar nacre formation, chitin appears and the chitin-binding Pif97 and N16 take action, exploiting the layer-forming ability of N16 shown here. In this hypothetical scenario, all three proteins (N16, Pif80, and Pif97) plus chitin concur to assemble the organic matrix layers in nacre and promote aragonite formation. The small yield of the N16N−aragonite lamellar crystals reported here highlights the need that these proteins have to work in concert and the difficulty in forming lamellar aragonite when only one protein or peptide is present. Suzuki et al. showed that removing only one of them stops lamellar nacre formation. We conclude that the *trio* of N16, Pif80, and Pif97 proteins, accompanied by chitin, are all necessary players, and none of them can form nacre *solo*.

Materials and Methods

Detailed preparations and methods are provided in the Supporting Information. We briefly describe here the sample growth and the X-PEEM performances.

(31) Schäffer, T. E.; Ionescu-Zanetti, C.; Proksch, R.; Fritz, M.; Walters, D. A.; Almqvist, N.; Zaremba, C. M.; Belcher, A. M.; Smith, B. L.; Stucky, G. D.; Morse, D. E.; Hansma, P. K. *Chem. Mater.* **1997**, *9*, 1731–1740.

(32) Towe, K. M.; Hamilton, G. H. *Calcif Tiss Internatl* **1967**, *1*, 306–318.

(33) Keene, E.; Evans, J. S.; Estroff, L. Langmuir 2009, *under review.*

In Vitro Mineralization. In vitro calcium carbonate growth was done in 10 mM $CaCl_2$ solutions exposed to ammonium carbonate [$(NH_4)_2CO_3$] vapors. The model biomineral systems were obtained by adding N16N or N16NN to a final concentration of 100 μM; negative controls included no additive.

X-PEEM. *P. fucata*, geologic calcite and aragonite crystals, and crystals grown in the presence of N16N, N16NN, or no peptide were embedded in epoxy, polished, and Pt coated for X-PEEM analysis on either the SPHINX or PEEM-3 microscopes, both of which are X-PEEM instruments, and these are not unique: X-PEEM instruments exist at most synchrotrons around the world, and access to them is usually granted to many inexperienced users, with full technical support and free of charge on the basis of a competitive scientific proposal selection. In an X-PEEM experiment, the sample is imaged while the illuminating photon energy is scanned. Each image pixel, therefore, contains the full X-ray absorption near-edge structure (XANES) spectrum across the C K-edge and Ca L-edge. XANES spectra are sensitive to the electronic structure surrounding the atom under analysis (Ca or C in this work). The spatial resolution can go down to 10 nm,[34] although for spectral analysis the probed area is usually larger (20 nm or greater) to reduce experimental noise.[27,30] Such analysis provides information on the presence and chemical state of elements in the sample, including relative concentration, crystal structure, and polymorphism (the $CaCO_3$ polymorphs calcite and aragonite are distinct in Figure 4, as are other crystals[35]). It can also distinguish amorphous from crystalline calcium carbonate and phosphate biominerals[27,30,36] and proteins from nucleic acids, lipids, and saccharides, although it cannot distinguish within these large classes of organic molecules.[37]

PIC Mapping. By acquiring X-PEEM images at a specific energy, the carbonate π^* peak at 290.3 eV in C spectra, and in combination with a linearly polarized illuminating X-ray beam, one produces PIC maps, in which gray level corresponds to crystal orientation with respect to the polarization vector. Although PIC mapping is extremely sensitive to the orientation of the *c*-axis in carbonate crystals, and misorientations as small as 2° can be detected with 10-nm resolution,[30] it is not at all sensitive to crystal rotation in the *ab*-plane.[29] Despite this limitation, PIC mapping proved valuable in the analysis of many carbonate biominerals because it is surface sensitive ($\sim$3 nm[29]) and the sample preparation does not require thinning or grinding; thus, it does not disrupt the spatial distribution and orientation of individual crystallites in a biomineral. Thus, PIC maps only probe one biomineral nanocomponent at a time in each image pixel, but they detect the relative orientation of many biomineral crystals in one 20-μm field of view, depending on the size of the crystal units, e.g., 400-nm thick $\times$5-μm wide tablets in nacre[29] or 10-nm particles in the matrix of the sea urchin tooth.[30]

Acknowledgment. We thank Doug B. Weibel and William L. Murphy for their help in sample preparation. This work was supported by NSF award DMR&CHE-0613972, DOE Award DE-FG02-07ER15899, UW-Vilas and Hamel Awards to P.U.P.A.G., and NSF award DMR-0906951 to S.N.C. The experiments were performed at the UW-SRC, supported by NSF award DMR-0537588, at the UW-Materials Science Center, also supported by NSF, and at the ALS supported by DOE under contract DE-AC02-05CH11231. Portions of this work were also supported by DoE award DE-FG02-03ER46099 to J.S.E., and this represents contribution 47 from the Laboratory for Chemical Physics, New York University.

Supporting Information Available: Detailed methods and two figures. This material is available free of charge via the Internet at http://pubs.acs.org.

JA909735Y

(34) Frazer, B. H.; Girasole, M.; Wiese, L. M.; Franz, T.; De Stasio, G. *Ultramicroscopy* **2004**, *99*, 87–94.
(35) Gilbert, B.; Frazer, B. H.; Belz, A.; Conrad, P.; Nealson, K. H.; Haskel, D.; Lang, J. C.; Srajer, G.; De Stasio, G. *J. Phys. Chem. A* **2003**, *107*, 2839–2847.
(36) Beniash, E.; Metzler, R. A.; Lam, R. S. K.; Gilbert, P. U. P. A. *J. Struct, Biol.* **2009**, *166*, 133–143.
(37) Chan, C. S.; De Stasio, G.; Welch, S. A.; Girasole, M.; Frazer, B. H.; Nesterova, M.; Fakra, S.; Banfield, J. F. *Science* **2004**, *303*, 1656–1658.
(38) Samata, T.; Hayashi, N.; Kono, M.; Hasegawa, K.; Horita, C.; Akera, S. *FEBS Lett.* **1999**, *462*.
(39) Miyashita, T.; Takagi, R.; Okushima, M.; Nakano, S.; Miyamoto, H.; Nishikawa, E.; Matsushiro, A. *Marine Biotechnology* **2000**, *2*, 409–418.